Letter

Effect of hole doping on superconductivity in compressed CeH_9 at high pressures

Chongze Wang,[1] Shuyuan Liu,[1] Hyunsoo Jeon,[1] Seho Yi,[1] Yunkyu Bang,[2,3] and Jun-Hyung Cho[1,3,*]

[1]*Department of Physics, Research Institute for Natural Science, and Institute for High Pressure at Hanyang University, Hanyang University, 222 Wangsimni-ro, Seongdong-Ku, Seoul 04763, Republic of Korea*

[2]*Department of Physics, Pohang University of Science and Technology, Pohang 37673, Republic of Korea*

[3]*Asia Pacific Center for Theoretical Physics, Pohang-si, Gyeongsangbuk-do 37673, Republic of Korea*

(Received 17 January 2021; revised 10 June 2021; accepted 17 June 2021; published 12 July 2021)

The experimental realization of high-temperature superconductivity in compressed hydrides H_3S and LaH_{10} under high pressures over 150 GPa has aroused great interest in reducing the stabilization pressure of superconducting hydrides. For cerium hydride CeH_9 recently synthesized at 80–100 GPa, our first-principles calculations reveal that the strongly hybridized electronic states of Ce-4f and H-1s orbitals produce the topologically nontrivial Dirac nodal lines around the Fermi energy E_F, which are protected by crystalline symmetries. By hole doping, E_F shifts down toward the symmetry-driven van Hove singularity to increase the density of states, which in turn significantly raises a superconducting transition temperature T_c. We show that hole doping with Ce^{3+} ions can be very electronically miscible in CeH_9 because both Ce^{3+} and Ce behave similarly as cations. Therefore, the interplay of crystalline symmetry, band topology, and hole doping contributes to enhance T_c in compressed CeH_9, which can also be demonstrated in another superconducting rare-earth hydride, LaH_{10}.

DOI: 10.1103/PhysRevB.104.L020504

Doping in condensed matters is a well-established means of manipulating their electronic structures, which may lead to the emergence of various quantum phases with exotic physical properties [1–7]. For example, in the unconventional high-temperature superconductors such as cuprates [8] and pnictides [9,10], doping by holes or electrons has been demonstrated not only to induce complex quantum phase transitions, but also to vary T_c in their superconducting phases [4–7]. However, identifying the mechanism responsible for the doping-induced changes of T_c in such unconventional superconductors has been elusive because of the emergence of many electronic states involved. By contrast, the effect of doping in conventional Bardeen-Cooper-Schrieffer [11] superconductors has been relatively well understood in terms of the influence of electron-phonon coupling (EPC), and therefore various dopants can be employed to tune T_c [12,13]. It is interesting and promising that the effects of doping on the EPC-driven superconductivity (SC) are expanded to be applicable to recently discovered hydrides under high pressures [14].

During the past six years, compressed hydrides under megabar pressures have attracted much attention because of their unprecedented records of T_c. Motivated by the theoretical predictions of SC in many hydrides [15–24], experiments have confirmed that sulfur hydride H_3S and lanthanum hydride LaH_{10} exhibit T_c around 203 K at ≈155 GPa [25] and 250–260 K at ≈170 GPa [26,27], respectively. More recently, carbonaceous sulfur hydride was experimentally realized to reach a room-temperature SC with $T_c = 288$ K at ≈267 GPa [28]. Nevertheless, it is highly demanding to discover high-T_c superconducting hydrides synthesized at moderate pressures below ≈100 GPa using a diamond anvil cell [29,30]. Near simultaneously, two experimental groups [31,32] reported the successful synthesis of cerium hydride CeH_9 at 80–100 GPa. The subsequent density-functional theory (DFT) calculation for CeH_9 revealed that the delocalized nature of Ce-4f electrons is an essential ingredient in the high chemical precompression of the clathrate H cage around the Ce atom [see Fig. 1(a)]. It is noticeable that, even though the synthesis of CeH_9 was made at lower pressures below ≈100 GPa, its theoretically predicted T_c value was around 75 K [21], much lower than those of H_3S and LaH_{10} [25–27]. Therefore, the main bottleneck for the research of high-T_c hydrides has been associated with difficulties both raising T_c and lowering the pressure of stability simultaneously. In order to alleviate this bottleneck in CeH_9, we here investigate the effect of hole doping on SC, which leads to a significant increase in T_c.

For clathrate-structured rare-earth superhydrides, the electronic states tend to have a strong hybridization between rare-earth-4f and H-1s orbitals near E_F [22,33–37]. This electronic characteristic of rare-earth hydrides having high-symmetry structures could be favorable for hosting topological states through band inversions, identified in recent studies of topological materials [38–43]. However, exploration of the cooperative interplay of crystal symmetry and band topology has been overlooked in high-pressure superconducting hydrides. These ingredients of symmetry and topology together with hole doping will provide a promising playground to enhance T_c in high-pressure superconducting hydrides, as will be demonstrated below.

In this Letter, using first-principles calculations, we discover that CeH_9 possessing a hexagonal-close-packed (hcp) structure has symmetry-enforced topologically

*Corresponding author: chojh@hanyang.ac.kr

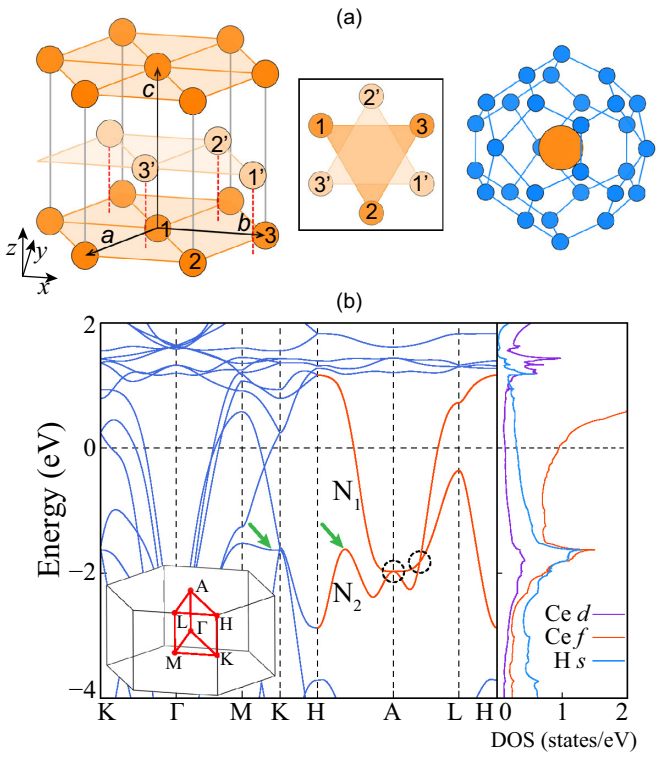

FIG. 1. (a) Optimized hcp structure of Ce atoms in CeH_9. The inset shows the top view of Ce atoms, and the isolated H_{29} cage surrounding a Ce atom is also included. The calculated band structure of CeH_9 together with the PDOS for Ce-4f, Ce-5d, and H-1s orbitals is given in (b). The unit of DOS is states/eV per unit cell that contains two Ce atoms. N_1 and N_2 represent the fourfold degenerate bands along the high-symmetry H-A-L-H paths, and the energy zero is E_F. The Brillouin zone of the hcp structure is also included in (b). The arrows in (b) represent the saddle point and partially flat band which mostly contribute the DOS peak of vHs.

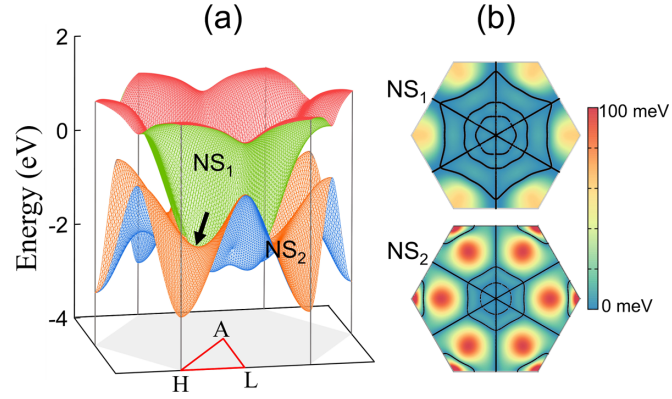

FIG. 2. (a) Energy of 2D nodal surfaces NS_1 and NS_2 throughout the $k_z = \pi/c$ plane, obtained without including SOC, and (b) 1D nodal lines converted from NS_1 and NS_2 with including SOC. In (a), one saddle point along the A-H line is marked by the arrow. In (b), the SOC-induced gap is represented using the color scale in the range between 0 and 100 meV.

nontrivial Dirac-nodal-line (DNL) states. It is revealed that the two-dimensional (2D) nodal surface guaranteed by the nonsymmorphic crystal symmetry S_{2z} (equivalent to the combination of twofold rotation symmetry C_{2z} about the z axis and a half translation along the z direction) is converted to one-dimensional (1D) DNLs in the presence of spin-orbit coupling (SOC) [44]. Moreover, such DNL states composed of strongly hybridized Ce-4f and H-1s orbitals lead to the formation of a van Hove singularity (vHs) around -1.6 eV below E_F. We propose that hole doping with Ce^{3+} ions shifts E_F toward the vHs, which in turn increases EPC and therefore raises T_c from 74 K (without hole doping) up to 136 K at 100 GPa. Our findings provide an avenue for using hole doping to enhance T_c in recently synthesized rare-earth hydrides CeH_9 [31,32] as well as LaH_{10} [26,27].

We first present the electronic band structure of hcp CeH_9, obtained using first-principles DFT calculations [45]. In most of the calculations hereafter, we fix a pressure of 100 GPa at which the hcp phase with the lattice parameters $a = b = 3.698$ Å and $c = 5.596$ Å [see Fig. 1(a)] is thermodynamically stable [see Fig. S1(a) in the Supplemental Material [58]]. It is noted that at 70 GPa the hcp phase becomes dynamically unstable with the presence of imaginary phonon frequencies [see Fig. S1(b) in [58]]. Figure 1(b) shows the calculated band structure and partial density of states (PDOS) of CeH_9. We find that the Ce-4f and H-1s orbitals are dominant components in the electronic states around E_F, compared to other orbitals (see Fig. S2 in [58]). Interestingly, the PDOS for Ce-4f and H-1s orbitals exhibits a sharp peak around -1.6 eV below E_F [see Fig. 1(b)], indicating a strong hybridization of the two orbitals. The existence of such a vHs having large DOS leads to an increase of T_c via hole doping, as discussed below.

Figure 1(b) represents the DFT band structure computed without including SOC. The presence of space-inversion symmetry P and time-reversal symmetry T ensures Kramers double degeneracy in the whole Brillouin zone (BZ). We find that there are fourfold degenerate bands N_1 and N_2 along the high-symmetry H-A-L-H paths, formed by touching of two bands. It is noted that N_1 and N_2 touch each other at A and between A and L [marked by dashed circles in Fig. 1(c)], thereby giving rise to eightfold accidental degeneracies. Using the tight-binding Hamiltonian with a basis of maximally localized Wannier functions [60,61], we reveal the existence of 2D nodal surfaces NS_1 and NS_2 throughout the $k_z = \pi/c$ plane, as shown in Fig. 2(a). Here, each nodal surface is formed by a touching of two doubly degenerate bands at the boundary of the BZ. Since the crystalline symmetry of hcp CeH_9 belongs to the space group $P6_3/mmc$ (no. 194) with the point group D_{6h}, the fourfold degeneracy of NS_1 and NS_2 is respected by the combined symmetry PS_{2z}, the eigenvalues of which are ± 1 because of $(PS_{2z})^2 = 1$ (see symmetry analysis in the Supplemental Material [58]). The inclusion of SOC lifts the degeneracy of N_1 and N_2 along the H-A-L-H paths except A-L (see Fig. S3 in [58]), where the SOC-induced gap opening is less than ≈ 0.1 eV [see Fig. 2(b)]. It is noted that the nodal surfaces NS_1 and NS_2 are converted into 1D nodal lines along the high-symmetry paths $k_x = 0$ and $k_x = \pm\sqrt{3}k_y$ as well as with circular patterns around the A point [see Fig. 2(b)]. These DNLs showing C_{3z} rotation symmetry are protected by additional mirror symmetry [62] (see symmetry analysis in the Supplemental Material [58]).

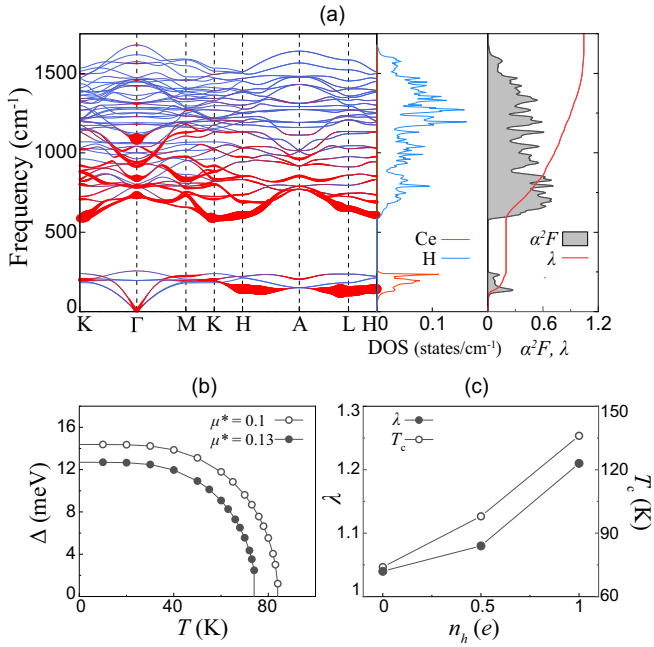

FIG. 3. (a) Calculated phonon spectrum, phonon DOS projected onto Ce and H atoms, Eliashberg function $\alpha^2F(\omega)$, and integrated EPC constant $\lambda(\omega)$ of CeH_9, (b) superconducting energy gap Δ as a function of temperature with $\mu^* = 0.1$ and 0.13, and (c) λ and T_c as a function of n_h.

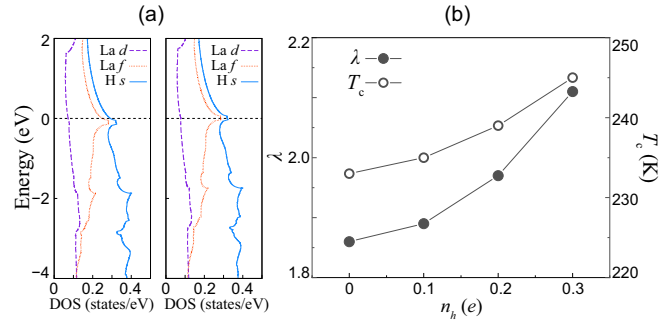

FIG. 4. (a) Calculated PDOS of LaH_{10}, obtained without hole doping (left) and at $n_h = 0.1e$ (right). The unit of DOS is states/eV per unit cell that contains one La atom. In (b), the calculated λ and T_c values are displayed as a function of n_h.

It is noteworthy that the vHs arises from the saddle points of energy dispersion [see Fig. 2(a)], located near the band touching of N_1 (NS_1) and N_2 (NS_2). There are six saddle points around the A point, one of which corresponds to the extremum point [marked by the arrow in Fig. 1(b)] along the A-H line. Moreover, the dispersion of this saddle point is rather flat in the k_z direction [see Fig. S4(a) in [58]], thereby leading to a major contribution to the DOS peak of vHs [see Fig. S4(b) in [58]]. In addition, the partially flat band [marked by the arrow in Fig. 1(b)] near the K point also gives some contribution to the DOS peak of vHs [see Fig. S4(b) in [58]]. The resulting vHs with a power law divergence in the DOS [63] in turn enhances T_c via hole doping, as discussed below. We note that there are numerous previous works about the influence of vHs or flat bands on SC. For examples, band engineering with utilizing various tricks such as twisted stacking of multilayer graphene [64,65] and strain-induced pseudomagnetic fields [66] increases the electronic DOS near E_F, thereby inducing the emergence of SC or enhancing T_c. It is also noteworthy that the high-T_c hydrides such as LaH_{10} and H_3S also have DNLs around E_F [33], which lead to the formation of vHs. Therefore, the vHs accompanied by symmetry-protected degeneracies is rather generic to high-T_c SC in compressed hydrides with high-symmetry structures.

To estimate T_c of CeH_9 at 100 GPa, we calculate the phonon spectrum, projected phonon DOS onto Ce and H atoms, Eliashberg function $\alpha^2F(\omega)$, and integrated EPC constant $\lambda(\omega)$ as a function of phonon frequency. Figure 3(a) shows that the phonon spectrum is divided into two regimes arising from Ce and H atoms, respectively [67]. By numerically solving the isotropic Migdal-Eliashberg equations [68–70], we calculate the superconducting gap versus temperature with varying Coulomb pseudopotential parameter μ^* [21,32], and estimate $T_c \approx 84$ and 74 K with $\mu^* = 0.1$ and 0.13, respectively [see Fig. 3(b)] [71]. These predicted T_c values of CeH_9 are much lower than the experimentally observed $T_c \approx 260$ K of LaH_{10} [26,27]. The lower T_c in CeH_9 is associated with relatively lower EPC constant compared to the case of LaH_{10} [33–35]. It is also noted that the H-derived DOS of CeH_9 at E_F is smaller than that of LaH_{10} [see Fig. 4(a)].

Since a vHs in the electronic DOS of CeH_9 is located below E_F [see Fig. 1(b)], hole doping is expected to induce a shift of E_F toward the vHs. The calculated band structure at a hole doping of $n_h = 1.0e$ per Ce atom shows that E_F approaches the vHs, thereby giving rise to an increase of DOS around E_F (see Fig. S5 in [58]). In order to examine how the hole doping influences SC, we use the isotropic Migdal-Eliashberg formalism [68–70] to estimate the variations of λ and T_c as a function of n_h. As shown in Fig. 3(c), λ is enhanced from 1.04 (without hole doping) to 1.08 and 1.21 at $n_h = 0.5$ and $1.0e$, respectively, which in turn increases T_c up to 136 K at $n_h = 1.0e$. It is thus likely that the increased DOS around E_F via hole doping increases the EPC channels, resulting in an increase of T_c [72]. Here, the hole doping with $n_h < 1.2e$ is found to preserve a structural stability without imaginary phonon frequencies (see Fig. S6 in [58]).

We here propose that the hole doping of CeH_9 can be achieved by the substitution of Ce^{3+} ions for Ce atoms. In order to examine the electronic miscibility of Ce^{3+} ions in the CeH_9 matrix, we calculate the charge density of CeH_9 without hole doping (see Fig. S7 in [58]). Interestingly, we find that the total charge inside the Ce muffin-tin sphere with radius 1.40 Å is $9.55e$ with including the $5s^25p^6$ semicore electrons [74], close to that ($9.63e$) obtained at $n_h = 1.0e$. This near invariance of Ce charges between the two systems implies that both Ce and Ce^{3+} behave similarly as cations. We note that Ce atoms in compressed CeH_9 become a strong cation due to an electride character of the isolated Ce framework (see Fig. S8 in [58]). It is thus likely that, when hole doping is formed in CeH_9 even with $n_h = 1.0e$ per Ce atom (equivalent to 33% Ce^{3+} ion concentration), Ce^{3+} and Ce would exhibit the same cationic states without hole localization around Ce^{3+} ions [77]. Based on our results for the charge distribution and structural stability of hole doping $n_h < 1.2e$, Ce^{3+} ions are most likely to be electronically miscible with Ce atoms in the

CeH_9 matrix. From an experimental point of view, since the Ce^{3+} ion is available with high stability in air [78], Ce^{3+} ion doping in compressed CeH_9 is anticipated to be experimentally realized in the future.

Finally, we also explore the effect of hole doping on SC in a recently observed [26,27] rare-earth hydride LaH_{10}. As shown in Fig. 4(a), the band structure of LaH_{10} computed at 300 GPa exhibits a vHs near E_F with a strong hybridization of La-4f and H-1s orbitals [33]. The calculated λ and T_c values of LaH_{10} are displayed as a function of n_h in Fig. 4(b). Since the DOS around E_F increases with hole doping [see Fig. 4(a)], λ increases monotonously with increasing n_h. Consequently, hole doped LaH_{10} raises T_c from 233 K (without hole doping) to 245 K at $n_h = 0.3e$ [79]. Here, the hole doping induced increase of T_c is 12 K, much smaller than the corresponding $\Delta T_c \approx 62$ K in CeH_9 [see Fig. 3(c)]. The relatively smaller value of ΔT_c in LaH_{10} is partly associated with the weak variation of DOS around E_F via hole doping [see Fig. 4(a)].

In summary, based on first-principles calculations, we proposed that hole doping significantly enhances T_c in a recently synthesized [31,32] hydride CeH_9. It was revealed that hole doping with Ce^{3+} ions induces the shift of E_F toward a vHs, thereby leading to the enhancement of EPC through an increased DOS around E_F. Interestingly, the vHs was found to be associated with the band touching of two crystalline symmetry-protected DNLs the electronic states of which are mostly composed of hybridized Ce-4f and H-1s orbitals. Therefore, the crystalline symmetry, band topology, and hole doping cooperate to increase T_c of compressed CeH_9. The proposed effect of hole doping on SC is rather generic and, hence, it can also be applicable to another experimentally observed [26,27] high-T_c rare-earth hydride, LaH_{10}. We anticipate that future experimental work will be stimulated to adopt hole doping for raising T_c in high-pressure superconducting hydrides.

This work was supported by the National Research Foundation of Korea (NRF) funded by the Korean Government (Grants No. 2019R1A2C1002975, No. 2016K1A4A3914691, and No. 2015M3D1A1070609). Y.B acknowledges an NRF grant funded by the Korean Government (Grant No. 2020-R1A2C2-007930). Calculations were performed by the KISTI Supercomputing Center through the Strategic Support Program (Program No. KSC-2021-CRE-0055) for supercomputing application research.

C.W. and S.L. contributed equally to this work.

[1] H. J. Queisser and E. E. Haller, Science **281**, 945 (1998).
[2] Y. Tokura, H. Takagi, and S. Uchida, Nature (London) **337**, 345 (1989).
[3] Y. Cao, V. Fatemi, S. Fang, K. Watanabe, T. Taniguchi, E. Kaxiras, and P. Jarillo-Herrero, Nature (London) **556**, 34 (2018).
[4] P. A. Lee, N. Nagaosa, and X.-G. Wen, Rev. Mod. Phys. **78**, 17 (2006).
[5] B. Keimer, S. A. Kivelson, M. R. Norman, S. Uchida, and J. Zaanen, Nature (London) **518**, 179 (2015).
[6] G. R. Stewart, Rev. Mod. Phys. **83**, 1589 (2011).
[7] P. Dai, Rev. Mod. Phys. **87**, 855 (2015).
[8] J. G. Bednorz and K. A. Müller, Z. Phys. B Condens. Matter **64**, 189 (1986).
[9] Y. Kamihara, H. Hiramatsu, M. Hirano, R. Kawamura, H. Yanagi, T. Kamiya, and H. Hosono, J. Am. Chem. Soc. **128**, 10012 (2006).
[10] Y. Kamihara, T. Watanabe, M. Hirano, and H. Hosono, J. Am. Chem. Soc. **130**, 3296 (2008).
[11] J. Bardeen, L. N. Cooper, and J. R. Schrieffer, Phys. Rev. **106**, 162 (1957).
[12] G. Profeta, M. Calandra, and F. Mauri, Nat. Phys. **8**, 131 (2012).
[13] G. Profeta, C. Tresca, and A. Sanna, in *GraphITA*, edited by V. Morandi and L. Ottaviano (Springer, New York, 2017), pp. 31–45.
[14] J. A. Flores-Livas, L. Boeri, A. Sanna, G. Profeta, R. Arita, and M. Eremets, Phys. Rep. **856**, 1 (2020), and references therein.
[15] E. Zurek, R. Hoffmann, N. W. Ashcroft, A. R. Oganov, and A. O. Lyakhov, Proc. Natl. Acad. Sci. USA **106**, 42 (2009).
[16] J. Hooper and E. Zurek, J. Phys. Chem. C **116**, 13322 (2012).
[17] H. Wang, J. S. Tse, K. Tanaka, T. Litaka, and Y. Ma, Proc. Natl. Acad. Sci. USA **109**, 6463 (2012).
[18] Y. Xie, Q. Li, A. R. Oganov, and H. Wang, Acta Cryst. C **70**, 104 (2014).
[19] D. Duan, Y. Liu, F. Tian, D. Li, X. Huang, Z. Zhao, H. Yu, B. Liu, W. Tian, and T. Cui, Sci. Rep. **4**, 6968 (2014).
[20] X. Feng, J. Zhang, G. Gao, H. Liu, and H. Wang, RSC Adv. **5**, 59292 (2015).
[21] F. Peng, Y. Sun, C. J. Pickard, R. J. Needs, Q. Wu, and Y. Ma, Phys. Rev. Lett. **119**, 107001 (2017).
[22] H. Liu, I. I. Naumov, R. Hoffmann, N. W. Ashcroft, and R. J. Hemley, Proc. Natl. Acad. Sci. USA **114**, 6990 (2017).
[23] Y. Sun, J. Lv, Y. Xie, H. Liu, and Y. Ma, Phys. Rev. Lett. **123**, 097001 (2019).
[24] H. Xie, Y. Yao, X. Feng, D. Duan, H. Song, Z. Zhang, S. Jiang, S. A. T. Redfern, V. Z. Kresin, C. J. Pickard, and T. Cui, Phys. Rev. Lett. **125**, 217001 (2020).
[25] A. P. Drozdov, M. I. Eremets, I. A. Troyan, V. Ksenofontov, and S. I. Shylin, Nature (London) **525**, 73 (2015).
[26] M. Somayazulu, M. Ahart, A. K. Mishra, Z. M. Geballe, M. Baldini, Y. Meng, V. V. Struzhkin, and R. J. Hemley, Phys. Rev. Lett. **122**, 027001 (2019).
[27] A. P. Drozdov, P. P. Kong, V. S. Minkov, S. P. Besedin, M. A. Kuzovnikov, S. Mozaffari, L. Balicas, F. F. Balakirev, D. E. Graf, V. B. Prakapenka, E. Greenberg, D. A. Knyazev, M. Tkacz, and M. I. Eremets, Nature (London) **569**, 528 (2019).
[28] E. Snider, N. Dasenbrock-Gammon, R. McBride, M. Debessai, H. Vindana, K. Vencatasamy, K. V. Lawler, A. Salamat, and R. P. Dias, Nature (London) **586**, 373 (2020).
[29] W. A. Bassett, High Press. Res. **29**, 163 (2009).
[30] H. K. Mao, X. J. Chen, Y. Ding, B. Li, and L. Wang, Rev. Mod. Phys. **90**, 015007 (2018).
[31] X. Li, X. Huang, D. Duan, C. J. Pickard, D. Zhou, H. Xie, Q. Zhuang, Y. Huang, Q. Zhou, B. Liu, and T. Cui, Nat. Commun. **10**, 3461 (2019).

[32] N. P. Salke, M. M. Davari Esfahani, Y. Zhang, I. A. Kruglov, J. Zhou, Y. Wang, E. Greenberg, V. B. Prakapenka, J. Liu, A. R. Oganov, and J.-F. Lin, Nat. Commun. **10**, 4453 (2019).
[33] L. Liu, C. Wang, S. Yi, K. W. Kim, J. Kim, and J.-H. Cho, Phys. Rev. B **99**, 140501(R) (2019).
[34] C. Wang, S. Yi, and J.-H. Cho, Phys. Rev. B **100**, 060502(R) (2019).
[35] C. Wang, S. Yi, and J.-H. Cho, Phys. Rev. B **101**, 104506 (2020).
[36] H. Jeon, C. Wang, S. Yi, and J.-H. Cho, Sci. Rep. **10**, 16878 (2020).
[37] D. A. Papaconstantopoulos, M. J. Mehl, and P.-H. Chang, Phys. Rev. B **101**, 060506(R) (2020).
[38] N. P. Armitage, E. J. Mele, and A. Vishwanath, Rev. Mod. Phys. **90**, 015001 (2018), and references therein.
[39] S. Liu, C. Wang, L. Liu, J.-H. Choi, H.-J. Kim, Y. Jia, C. H. Park, and J.-H. Cho, Phys. Rev. Lett. **125**, 187203 (2020).
[40] Y. Kim, B. J. Wieder, C. L. Kane, and A. M. Rappe, Phys. Rev. Lett. **115**, 036806 (2015).
[41] C. Fang, Y. Chen, H.-Y. Kee, and L. Fu, Phys. Rev. B **92**, 081201(R) (2015).
[42] G. Bian, T.-R. Chang, R. Sankar, S.-Y. Xu, H. Zheng, T. Neupert, C.-K. Chiu, S.-M. Huang, G. Chang, I. Belopolski *et al.*, Nat. Commun. **7**, 10556 (2016).
[43] C. Fang, H. Weng, X. Dai, and Z. Fang, Chin. Phys. B **25**, 117106 (2016).
[44] Q.-F. Liang, J. Zhou, R. Yu, Z. Wang, and H. Weng, Phys. Rev. B **93**, 085427 (2016).
[45] Our DFT calculations were performed using the Vienna *ab initio* simulation package with the projector-augmented wave method [46–48]. For the exchange-correlation energy, we employed the generalized-gradient approximation functional of Perdew-Burke-Ernzerhof [49]. The $5s^25p^6$ semicore electrons of Ce atom were included in the electronic-structure calculations. A plane-wave basis was used with a kinetic energy cutoff of 1000 eV. The **k**-space integration was done with the $18\times18\times12$ k points for the structure optimization and the $48\times48\times32$ k points for the DOS calculation. All atoms were allowed to relax along the calculated forces until all the residual force components were less than 0.001 eV/Å. The phonon spectrum and EPC calculations were carried out by using the QUANTUM ESPRESSO package [50] with the norm-conserved Hartwigsen-Goedecker-Hutter pseudopotentials [51], a kinetic energy cutoff of 1224 eV, and the $3\times3\times2$ q and $18\times18\times12$ k points for the computation of phonon frequencies. For the calculation of EPC, we used the software EPW [52,53] with the $24\times24\times16$ q and $48\times48\times32$ k points. Using the DFT $+U$ calculation [54] with the Hubbard parameter $U = 4.5$ eV and exchange interaction parameter $J = 0.5$ eV, we found that the energy dispersion of electronic states around E_F changes little with respect to U (see Fig. S9 in the Supplemental Material [58]). We also performed the hybrid calculation with the HSE functional [55,56] to demonstrate that the dispersion of hybridized Ce-4f and H-1s states around E_F is nearly the same as the corresponding DFT result (see Fig. S10 in the Supplemental Material [58]). This HSE result together with the DFT $+U$ one (see Fig. S9 in [58]) convincingly confirms the validity of the present DFT calculation. Moreover, according to the experimental work [57] performed by Chen *et al.*, several CeH_9 samples exhibit T_c ranging between 73 and 97 K at ≈100 GPa, in good agreement with our predicted T_c values of 74–84 K using DFT calculation. These theoretical results together with the experimental data demonstrate that the present DFT calculation properly describes the SC observed in compressed CeH_9 and therefore correction effect on the Ce f orbitals is likely minor.
[46] G. Kresse and J. Hafner, Phys. Rev. B **48**, 13115 (1993).
[47] G. Kresse and J. Furthmüller, Comput. Mater. Sci. **6**, 15 (1996).
[48] P. E. Blöchl, Phys. Rev. B **50**, 17953 (1994).
[49] J. P. Perdew, K. Burke, and M. Ernzerhof, Phys. Rev. Lett. **77**, 3865 (1996); **78**, 1396(E) (1997).
[50] P. Giannozzi, S. Baroni, N. Bonini, M. Calandra, R. Car, C. Cavazzoni, D. Ceresoli, G. L. Chiarotti, M. Cococcioni, I. Dabo *et al.*, J. Phys.: Condens. Matter **21**, 395502 (2009).
[51] C. Hartwigsen, S. Goedecker, and J. Hutter, Phys. Rev. B **58**, 3641 (1998).
[52] F. Giustino, M. L. Cohen, and S. G. Louie, Phys. Rev. B **76**, 165108(R) (2007).
[53] S. Poncé, E. R. Margine, C. Verdi, and F. Giustino, Comput. Phys. Commun. **209**, 116 (2016).
[54] S. L. Dudarev, G. A. Botton, S. Y. Savrasov, C. J. Humphreys, and A. P. Sutton, Phys. Rev. B **57**, 1505 (1998).
[55] J. Heyd, G. E. Scuseria, and Z. Ernzerhof, J. Chem. Phys. **118**, 8207 (2003).
[56] A. V. Krukau, O. A. Vydrov, A. F. Izmaylov, and G. E. Scuseria, J. Chem. Phys. **125**, 224106 (2006).
[57] W. Chen, D. V. Semenok, X. Huang, H. Shu, X. Li, D. Duan, T. Cui, and A. R. Oganov, arXiv:2101.01315.
[58] See Supplemental Material at http://link.aps.org/supplemental/10.1103/PhysRevB.104.L020504 for symmetry and topology analyses, phonon frequencies, band projections onto the orbitals of Ce and H atoms, charge density plot with including the electron localization function [59], band structures computed with including SOC and U, and band structures obtained using hybrid and all-electron calculations.
[59] B. Silvi and A. Savin, Nature (London) **371**, 683 (1994).
[60] A. A. Mostofi, J. R. Yates, Y.-S. Lee, I. Souza, D. Vanderbilt, and N. Marzari, Comput. Phys. Commun. **178**, 685 (2008).
[61] Q. S. Wu, S. N. Zhang, H.-F. Song, M. Troyer, and A. A. Soluyanov, Comput. Phys. Commun. **224**, 405 (2018).
[62] For example, M_x: $(x, y, z) \to (-x, y, z)$ anticommuting with PS_{2z} allows the existence of the fourfold degenerate nodal line at $k_x = 0$ on the $k_z = \pi/c$ plane. The topological characterizations of these DNLs are demonstrated by calculating the topological index [43], defined as $\zeta_1 = \frac{1}{\pi}\oint_c dk A(k)$, along a closed loop encircling any of the DNLs. Here, $A(k) = -i\langle u_k \mid \partial_k \mid u_k\rangle$ is the Berry connection of the related Bloch bands. We obtain $\zeta_1 = \pm1$ for the DNLs, indicating that they are stable against PS_{2z} and M symmetries conserving perturbations.
[63] N. F. Q. Yuan, H. Isobe, and L. Fu, Nat. Commun. **10**, 5769 (2019).
[64] Y. Cao, V. Fatemi, S. Fang, K. Watanabe, T. Taniguchi, E. Kaxiras, and P. Jarillo-Herrero, Nature (London) **556**, 43 (2018).
[65] M. Yankowitz, S. Chen, H. Polshyn, Y. Zhang, K. Watanabe, T. Taniguchi, D. Graf, A. F. Young, and C. R. Dean, Science **363**, 1059 (2019).
[66] E. Tang and L. Fu, Nat. Phys. **10**, 964 (2014).
[67] It is noted that the Ce phonon modes contribute to ≈19% of the total EPC constant $\lambda = \lambda(\infty)$, whereas the H phonon

modes contribute to ≈81% of λ. Specifically, the H-derived low-frequency optical modes show larger EPC strength, as represented by circles on the phonon dispersion in Fig. 3(a). Therefore, the optical vibrations of H atoms are strongly coupled to the hybridized electronic states of Ce-4f and H-1s orbitals around E_F, giving rise to $\lambda = 1.04$.

[68] A. B. Migdal, Sov. Phys. JETP **34**, 996 (1958).

[69] G. M. Eliashberg, Sov. Phys. JETP **11**, 696 (1960).

[70] P. B. Allen and B. Mitrović, Solid State Phys. **37**, 1 (1983).

[71] The band dispersion of electronic states around E_F shows little change with respect to the absence [see Fig. 1(b)] and presence (see Fig. S3 in the Supplemental Material [58]) of SOC. Therefore, we can say that SOC hardly affects T_c in CeH_9.

[72] From McMillan's strong coupling theory [73], the EPC constant can be expressed by $\lambda = N(E_F)\cdot\langle I^2\rangle/(M\omega^2)$, where $N(E_F)$ is the density of states at the Fermi energy, $\langle I^2\rangle$ is the Fermi surface average of the square of the electron-phonon matrix element, and M and ω are the effective atomic mass and phonon frequency that reflect the role of the different atomic species and phonon vibrations involved in SC. Therefore, the H-derived electronic states dominantly contribute to increase λ, due to their larger values of I. As shown in Fig. 1(c), the DOS of H-derived electronic states exhibit a monotonous increase with approaching the vHs, thereby enhancing T_c via hole doping.

[73] W. L. McMillan, Phys. Rev. **167**, 331 (1968).

[74] It is noted that, unlike the highly localized $5s^2$ semicore state at around −35 eV below E_F, the $5p^6$ semicore states around −19 eV are well delocalized to hybridize with the H 1s state (see Fig. S9 in the Supplemental Material [58]). These band dispersions of semicore electrons are in good agreement with those obtained using all-electron calculation with the Fritz-Haber-Institute *ab initio* molecular simulations (FHI-AIMS) code [75] (see Fig. S11 in the Supplemental Material [58]). This delocalized feature of $5p^6$ semicore states in CeH_9 is similar to that in LaH_{10}, previously obtained using the PAW [76] and LAPW [37] calculations.

[75] V. Blum, R. Gehrke, F. Hanke, P. Havu, V. Havu, X. Ren, K. Reuter, and M. Scheffler, Comput. Phys. Commun. **180**, 2175 (2009).

[76] S. Yi, C. Wang, H. Jeon, and J.-H. Cho, Phys. Rev. Mater. **5**, 024801 (2021).

[77] We note that in the present calculations the hole charges are compensated by uniform background charge to maintain charge neutrality, as implemented in the VASP code [46,47]. This simulation of hole doping is believed to properly describe the incorporated Ce^{3+} ions in the CeH_9 matrix, because both Ce and Ce^{3+} with the same cation characters can be equally screened by their surrounding anionic H cages.

[78] T. Naganuma and E. Traversa, Nanoscale **4**, 4950 (2012).

[79] In our previous DFT calculation for LaH_{10} [33–35], $\alpha^2F(\omega)$ and $\lambda(\omega)$ showed that most of the phonon modes in the whole frequencies contribute to EPC. Therefore, the electronic states around E_F within an energy range of $\pm\hbar\omega_D$ (where ω_D is Debye frequency) are involved in the formation of Cooper pairing. As shown in Fig. S12 in the Supplemental Material [58], the magnitude of integrated DOS within $E_F \pm \hbar\omega_D$ increases with increasing n_h due to the asymmetry of DOS for the occupied and unoccupied states. These variations of DOS with respect to n_h are most likely to be associated with monotonic increases in λ and T_c [see Fig. 4(b)].